Article

Efficient Multifunctional Catalytic and Sensing Properties of Synthesized Ruthenium Oxide Nanoparticles

Ruby Phul [1], **Mohammad Perwez [2]**, **Jahangeer Ahmed [3]**, **Meryam Sardar [2]**,
Saad M. Alshehri [3], **Norah Alhokbany [3]**, **Mohd A. Majeed Khan [4]** and **Tokeer Ahmad [1],***

[1] Nanochemistry Laboratory, Department of Chemistry, Jamia Millia Islamia, New Delhi 110025, India; rubyphul@gmail.com

[2] Enzyme Technology Laboratory, Department of Biosciences, Jamia Millia Islamia, New Delhi 110025, India; perwezmohammad@gmail.com (M.P.); msardar@jmi.ac.in (M.S.)

[3] Department of Chemistry, College of Science, King Saud University, Riyadh 11451, Saudi Arabia; jahmed@ksu.edu.sa (J.A.); alshehri@ksu.edu.sa (S.M.A.); nhokbany@ksu.edu.sa (N.A.)

[4] King Abdullah Institute for Nanotechnology, King Saud University, Riyadh 11451, Saudi Arabia; mmkhan@ksu.edu.sa

* Correspondence: tahmad3@jmi.ac.in; Tel.: +91-11-26981717 (ext. 3261); Fax: +91-11-26980229

check for updates

Abstract: Ruthenium oxide is one of the most active electrocatalyst for oxygen evolution (OER) and oxygen reduction reaction (ORR). Herein, we report simple wet chemical route to synthesize RuO_2 nanoparticles at controlled temperature. The structural, morphological and surface area studies of the synthesized nanoparticles were conducted with X-ray diffraction, electron microscopy and BETsurface area studies. The bifunctional electrocatalytic performance of RuO_2 nanoparticles was studied under different atmospheric conditions for OER and ORR, respectively, versus reversible hydrogen electrode (RHE) in alkaline medium. Low Tafel slopes of RuO_2 nanoparticles were found to be ~47 and ~49 mV/dec for OER and ORR, respectively, in oxygen saturated 0.5 M KOH system. Moreover, the catalytic activity of RuO_2 nanoparticles was examined against the Horseradish peroxidase enzyme (HRP) at high temperature, and the nanoparticles were applied as a sensor for the detection of H_2O_2 in the solution.

Keywords: ruthenium oxide; nanoparticles; electrocatalysts; sensing

1. Introduction

The present generation is largely dependent on fossil fuelsto meet the present energy requirements—for instance, oil, coal, or natural gases. However, these energy demands fulfilled by these products directly affect the environment. The burning of fossil fuels leads up to the emissions of carbon dioxide gas (a greenhouse gas), which is affecting the world significantly through global warming, change in weather patterns and several other noteworthy geographical changes [1]. In addition, we know fossil fuels are nonrenewable resources, hence they will eventually deplete, so alternatives must be found. Therefore, the development of efficient, inexpensive and eco-friendly sources of energy has become a significant and crucial task for the researchers [2]. Scientists have investigated the use of renewable resources such as solar, wind, tidal, biomass, geothermal energy etc. The major research trend of today's era is the water-splitting phenomena for energy generation. Water splitting via electrocatalysis or photocatalysis is a clean, environmentally friendly and renewable source of energy for fuel cells, batteries and hydrogen generation [3–5]. In the presence of electro/photocatalyst, the water molecule splits into hydrogen and oxygen gas (i.e., $H_2O \rightarrow H_2 + 1/2 O_2$). The evolved

hydrogen gas is used in fuel cells as a fuel which further reacts with O_2 to produce an electric current. The evolved oxygen gas participates in the combustion reaction of fuel cells to generate power.

Forthe past few decades, researchers made headway in creating robust and efficient catalysts for the oxidation of water. Several noble metals viz. Pt, Ir, Ru and their oxide-based catalysts have been developed for oxidation–reduction reactions [6–8]. Various other earth-abundant metal-based catalysts such as Mn, Fe, Co, Cu and W were also reported for their role in water splitting reactions [9–13]. In a previous research era, stupendous research has been done in the fabrication of active electrode material for oxygen evolution reactions (OERs). The main limitation with this method is that the OER at the anode gives rise to a high energy loss. Therefore, the emphasis has been given on attaining a high oxygen evolution rate at a low overpotential by optimizing the overall water splitting reaction. Electrode corrosion and low current densities are also the major disadvantages of conventional anode materials for OER [14]. Currently, ruthenium oxide has been used in the fabrication of dimensionally stable anodes (DSA), which havebeen employed to yield chlorine [15]. In addition, it has been used as a heterogeneous catalyst for the low temperature dehydrogenation of NH_3 [16], HCl [17], and methanol [18], respectively. Further, ruthenium oxide was reported to work as anexcellent electrode material for OERs [19,20] and hydrogen evolution reactions (HERs) [21,22]. The metallic conductivity of RuO_2, along with IrO_2,is of the order of 10^4 ohm^{-1}cm^{-1} [23]. IrO_2 shows high corrosion-resistance, whereas RuO_2 shows better OER activity [24]. Among all the other transition metal oxides, RuO_2 and IrO_2 are considered as the best electrocatalytic materials for electrolysis of water in acidic as well as an alkaline mediums [25,26].

In the past few years, nanocrystalline RuO_2 particles were synthesized by thermal evaporation [27], nanocasting [28], cryogenic decomposition of RuO_4 [29] and electro-spinning [30]. Recently, M. P. Browne et al. [31] synthesized a series of $Mn_xO_y/RuO_2/Ti$ mixed oxide anode materials via a thermal decomposition method for OERs in alkaline medium. They have shown that electrocatalysts were containing different concentrations of Mn viz. 10%, 25% and 90% show almost similar or improved OER activity as compared to pure RuO_2. Gustafson et al. [32] have synthesized RuO_2 nanocatalyst for chemical and photochemical oxidation of water, which showed better catalytic performance as reported in the literature.

Presently, the artificial enzymes, i.e., nanoenzymes, are receiving significant attention of researchers due to their low cost, high catalytic property and thermal stability as compared to the natural enzymes. Prototypically, Gao et al. discovered that magnetite nanoparticles exhibit intrinsic peroxidase-like activity similar to that of a natural peroxidase enzyme [33]. H_2O_2 plays a vital role as an intermediate in food, pharmaceutical, clinical, and environmental analysis [34–36]. So, the detection of H_2O_2 has been done by using different nanoparticles. Besides that, H_2O_2 possesses a strong oxidizing property which may lead to different types of disorders in the body [37–39]. Hence, the detection of hydrogen peroxide is of a great practical feature.

Herein, we report the redox reaction of water (OER/ORR) happening through as-synthesized ruthenium oxide nanoparticles in 0.5M KOH electrolytic solution at room temperature under different atmospheres (air, N_2 and O_2). Further, the as-synthesized ruthenium oxide nanoparticles were also used as a sensor for the detection of H_2O_2 in solution. Moreover, the synthesis of RuO_2 nanoparticles was carried out through a simple, environmentally friendly and cost-effective wet chemical method at 80 °C followed by annealing at 300 °C for 6h.

2. Results and Discussion

The powder X-ray diffractometry was used for the structural analysis of the as-synthesized nanoparticles. Figure 1a shows the X-ray diffraction pattern of the nanocrystalline RuO_2. The obtained diffraction peaks are as follows at Bragg's angles of 27.8°, 34.9°, 39.8°, 54.0°, 57.6°, 59.2°, 65.2°, 66.7°, 69.2°, 73.8°, 82.9° and 87.3° corresponds to the planes (110), (101), (200), (211), (220), (002), (310), (112), (301), (202), (321) and (222), respectively, which were correlated to a tetragonal unit cell of ruthenium oxide. The reflection pattern could be indexed to a pure tetragonal phase of RuO_2(JCPDS No. 065-2824).

No peaks from any impurity or other phase or metallic Ru were detected, which affirms the formation of monophasic RuO_2 nanoparticles.

The microstructure and surface texture of as-synthesized ruthenium oxide nanoparticles wereinvestigated through SEM studies. Figure 1b shows the SEM micrograph of the as-synthesized nanoparticles. Further analysis of the SEM micrograph depicted the highlydense and agglomerated RuO_2 nanoparticles. The nanoparticles aggregate randomly to form almost spherical shape with an average diameter of 28 nm, which is as per the TEM analysis.
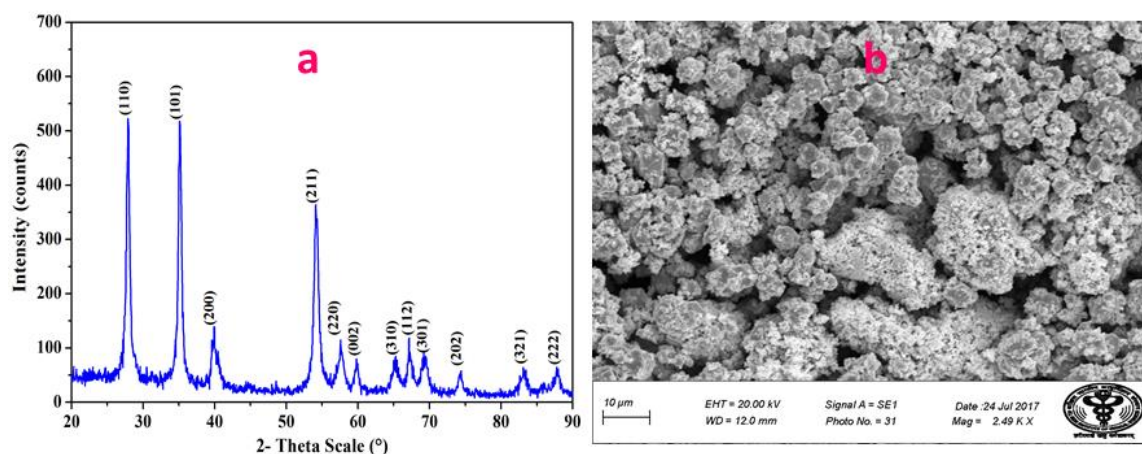

Figure 1. (**a**) X-ray diffraction pattern and (**b**) scanning electron microscope (SEM) micrograph of Ruthenium oxide nanoparticles.

The detailed structural analysis, shape and size distribution of RuO_2 nanoparticles was done with the help of TEM studies. The low magnification TEM micrograph is shown in Figure 2a, which indicates the formation of tiny sized tetragonal RuO_2 nanoparticles with slight agglomeration. Figure 2a also reveals that the small-sized nanoparticles tend to form large tetragonal structures, which are in accordance with X-ray diffraction studies. Furthermore, High Resolution Transmission Electron Microscope (HRTEM) analysis revealed the crystal structure, phase and growth direction of as-synthesized nanoparticles. Figure 2b shows the typical HRTEM image of ruthenium oxide nanoparticles, which depicts the well-resolved lattice fringes with an average lattice distance of 3.210 ± 0.05 Å and 2.560 ± 0.05 Å corresponding to (110) and (101) planes, respectively, of ruthenium oxide nanoparticles. The TEM average size distribution histogram of ruthenium oxide nanoparticles are shown in Figure 2c, which indicates that the particle size ranges from 5 nm to 35 nm, as the various small particles have combined to form a single massive particle. The average grain size was found to be ~20nm by using TEM micrograph as well as a size distribution plot.
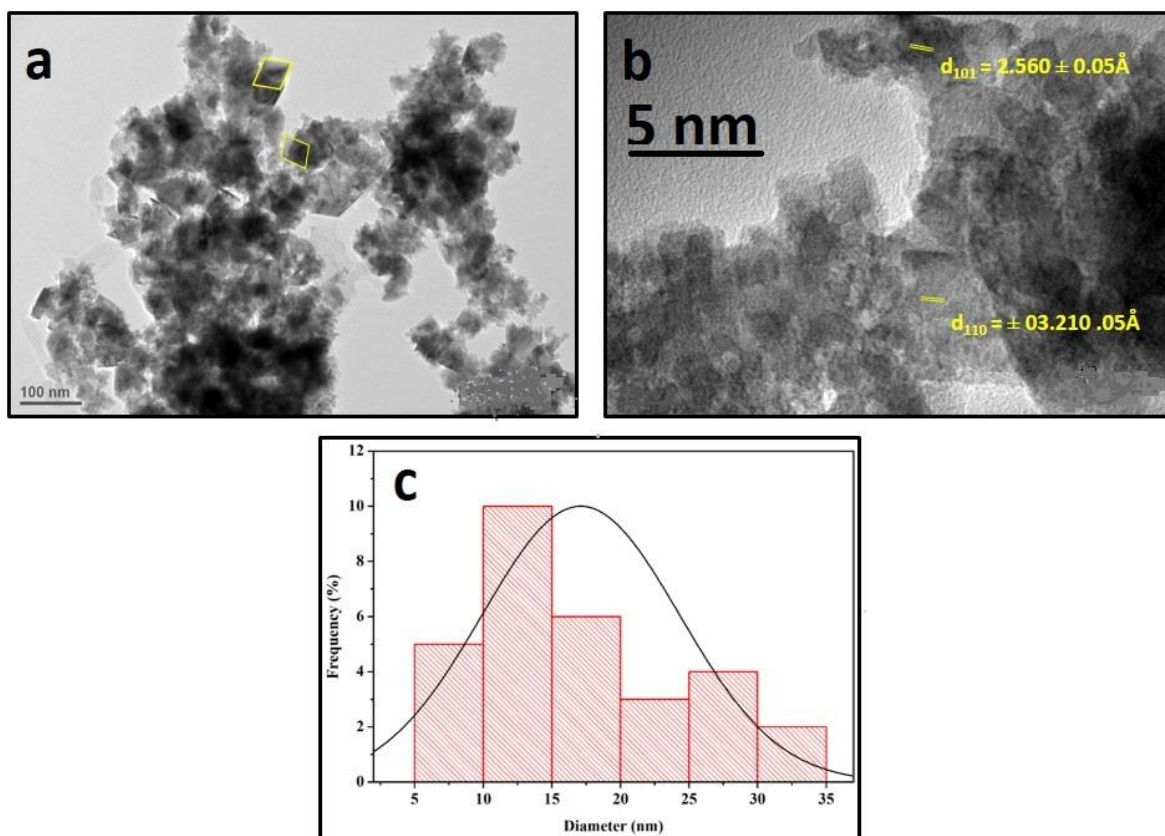
Figure 2. (**a**) TEM micrograph, (**b**) HR-TEM image and (**c**) size distribution histogram of Ruthenium oxide nanoparticles.

The specific surface area of as-prepared RuO_2 nanoparticles was estimated by using a multipoint BET equation that showed the linear relationship in the P/P_0 range of 0.05–0.35. Figure 3a shows the BET plot for RuO_2 nanoparticles. The specific surface area was found to be 64.5 m^2g^{-1}, which agrees with the earlier reported value [19]. The BJH (Barrett-Joyner-Halenda) model was used to determine the pore size. The pore size distribution plot of ruthenium oxide nanoparticles (Figure 3b) gives the pore radius value of 16 Å, which lies in the range of mesoporous materials. The pore radius was also determined by the DA (Dubinin-Astakhov) plot, as shown in Figure 3c, and it was found to be 13.5 Å, which is a bit smaller than the BJH results.
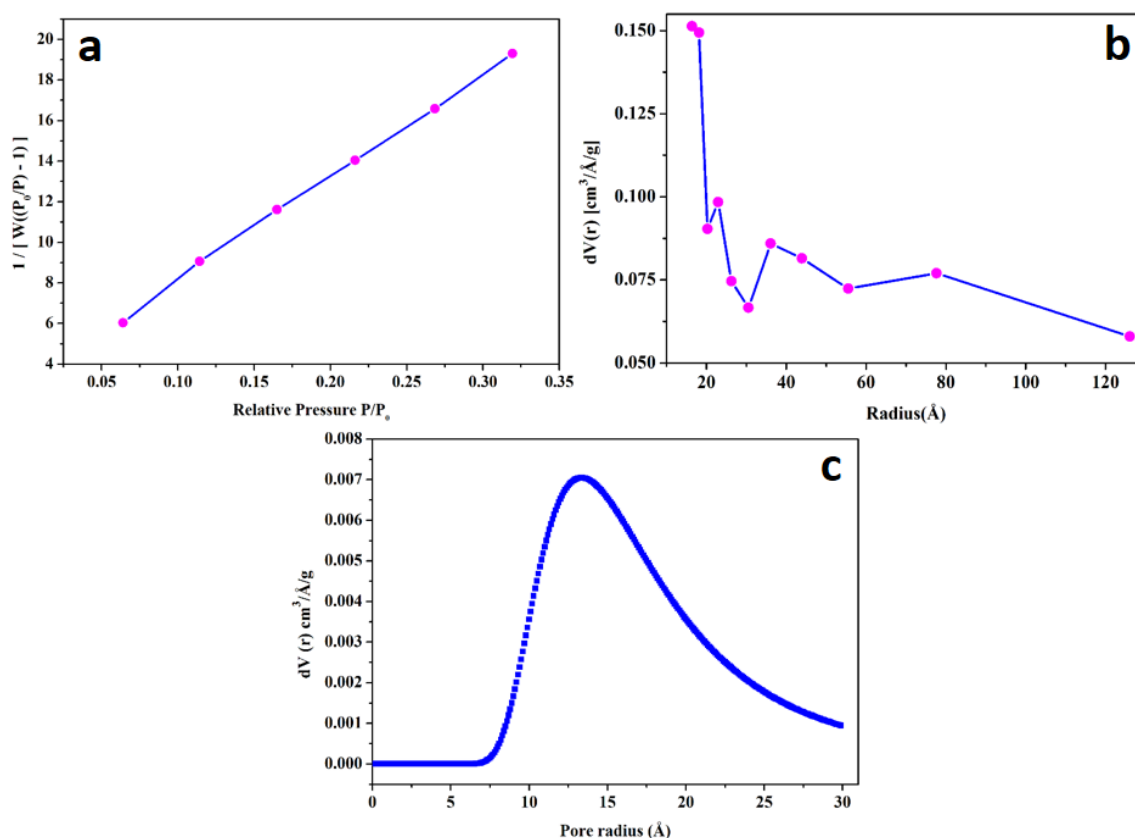
Figure 3. (**a**) BET, (**b**) BJH and (**c**) DA pore radius plots of ruthenium oxide nanoparticles.

The electrocatalytic activity of as-prepared nanoparticles for oxygen evolution reaction (OER) and oxygen reduction reaction (ORR) was evaluated by cyclic voltammetry (CV), linear sweep voltammetry (LSV) and Tafel polarization curves in 0.5M KOH electrolyte solution. The CV plots for OER (anodic sweep) and ORR (cathodic sweep) by ruthenium oxide electrode at the scan rate of 25 mVs^{-1} in the air (black), N_2 (red) and saturated O_2 (blue) atmosphere are shown in Figure 4a. The CV curves show that the OER starts from the low potential value of ~1.5 V vs. RHE (reversible hydrogen electrode). Figure 4a shows that the as-synthesized RuO_2 nanoparticles generate more current in O_2 saturated (17.5 mAcm^{-2}) as compared to air (11.5 mAcm^{-2}) and N_2 (10.5 mAcm^{-2}) atmosphere at 1.55 V vs. RHE at 25 mVs^{-1} for the oxygen evolution reaction. The ORR activity of ruthenium oxide nanoparticles in alkaline medium is also shown in Figure 4a. It was observed that as-synthesized RuO_2 nanoparticles show an almost comparable ORR reaction in all the atmospheric conditions. The LSV measurements optimized the electrocatalytic activity of ruthenium oxide nanoparticles in 0.5M KOH electrolyte at the scan rate of 25 mVs^{-1}. Figure 4b shows the LSV curves under air, nitrogen and O_2 saturated atmospheres. It was observed that the onset potential for OER was found to be ~1.5 (O_2) and ~1.61 V (air and N_2) vs. RHE. Notably, the resulting current density (current/area of the electrode) of RuO_2 electrode is directly related to the amount of oxygen evolved from the electrolysis of water. The geometric electro-active surface area of the working electrode could be estimated from the Randles–Sevik equation [40]. The current density of RuO_2 electrode at ~1.7 V versus RHE at 25 mVs^{-1} was found to be ~9.6 mAcm^{-2} (in N_2), ~11.9 mAcm^{-2} (in air) and ~15.5 mAcm^{-2} (in O_2). The significance of LSV measurements is to find the onset potential, reaction kinetics and mechanism of the reaction, i.e., to identify the number of electrons taking part in the electrochemical reaction. Figure 4c shows the LSV curves of RuO_2 nanoparticles for the oxygen reduction reaction in air, N_2, and O_2 saturated 0.5M KOH at the scan rate of 25 mVs^{-1}. From this study, we clearly observed that the ORR activity performed significantly better in an O_2-saturated system compared to other systems

as expected. The ORR activity in air could be due to the dissolved oxygen in system. Note that very weak ORR activity in N_2 was also observed, which could be due to the presence of oxygen content (5%) in N_2. The onset potential for ORR was found to be 0.7 V vs. RHE. Choronoamperometric (CA) measurements demonstrated the stability and the electrocatalyticactivity of the ruthenium oxide electrode at a fixed potential (1.5V vs. RHE) in O_2-saturated 0.5M KOH for 200 s. Figure 4d shows the CA curves, which demonstrate that the material is stable, and the constant current is generated with time. It was observed that the resulting current densities were consistent with time. The CA experiments also showed that on turning off the potential, the water redox reaction was stopped instantly, and therefore the current density dropped to zero. The current density obtained was directly proportional to the amount of gas evolved during the OER. The surface area of the electrode material used, and the Faradaic and Non-Faradaic processes were responsible for the resulting current density.
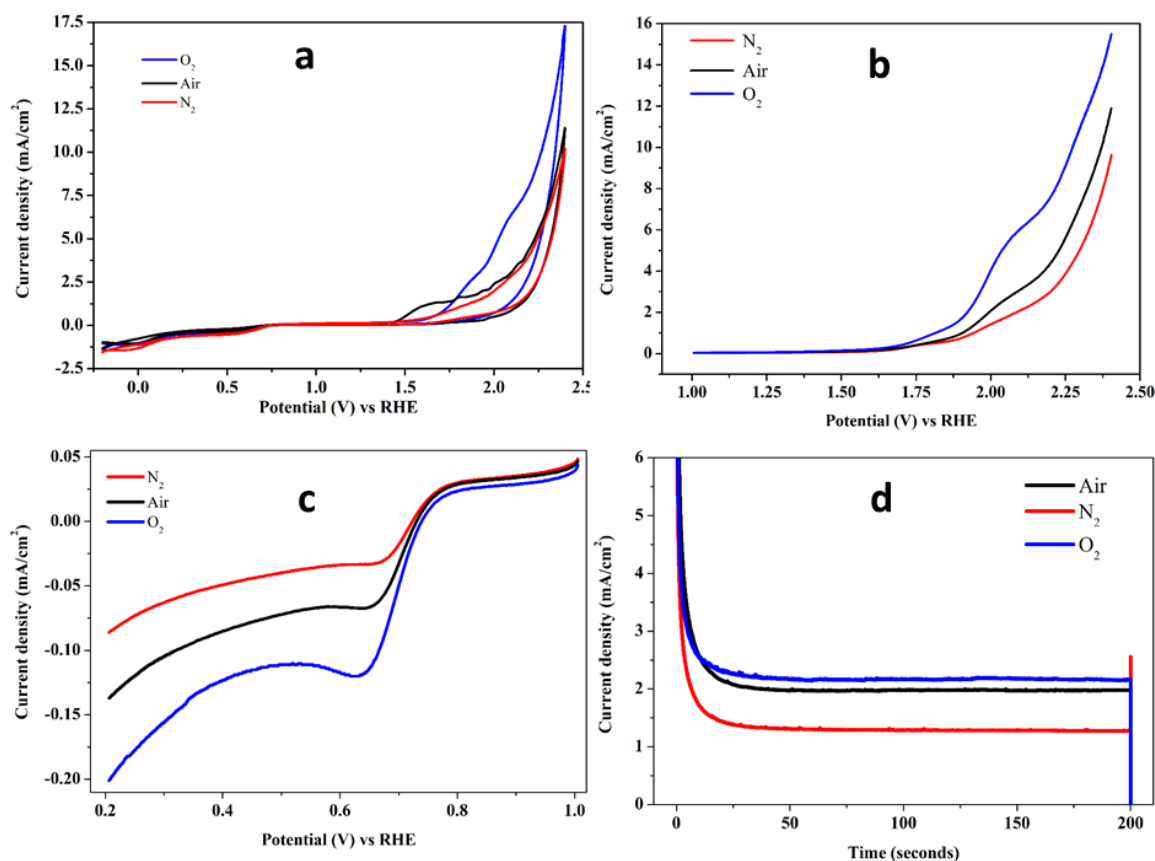

Figure 4. (**a**) CV, (**b**) LSV (OER), (**c**) LSV (ORR) curves of Ruthenium oxide photoanode in air, N_2 and O_2 saturated 0.5M KOH electrolyte vs. RHE at the scan rate of 25 mVs^{-1} and (**d**) CA curves of Ruthenium oxide nanoparticles for OER activity at 1.5 V vs. RHE in O_2-saturated 0.5M KOH.

The Tafel polarization studies determined the kinetics of the reaction, i.e., electrolysis of water. It was observed that reaction kinetics strongly depends upon the size, surface area, morphology and orientation of electrocatalysts [14,41]. Figure 5a,b shows the Tafel polarization plot of ruthenium oxide nanoparticles for the water redox reactions (OER and ORR) in air, and O_2, respectively. The linear curve fitting calculated the value of Tafel slopes of ruthenium oxide nanoparticles, and it comes out to be 76, and 47 mVdec^{-1} in air, and O_2, respectively, for OER while for ORR, these values were found to be 48 (air), and 49 mVdec^{-1} (O_2) with the experimental error of ±5. The effective electro-active catalysts for water splitting could lower the Tafel slope values to sustain the high activity, stability and to enhance the efficiency by reducing the loss of energy during the electrochemical reactions [42].

The comparison in the current electrocatalytic activities viz. OER/ORR of RuO_2 nanoparticles with the literature has been tabulated in Table 1.
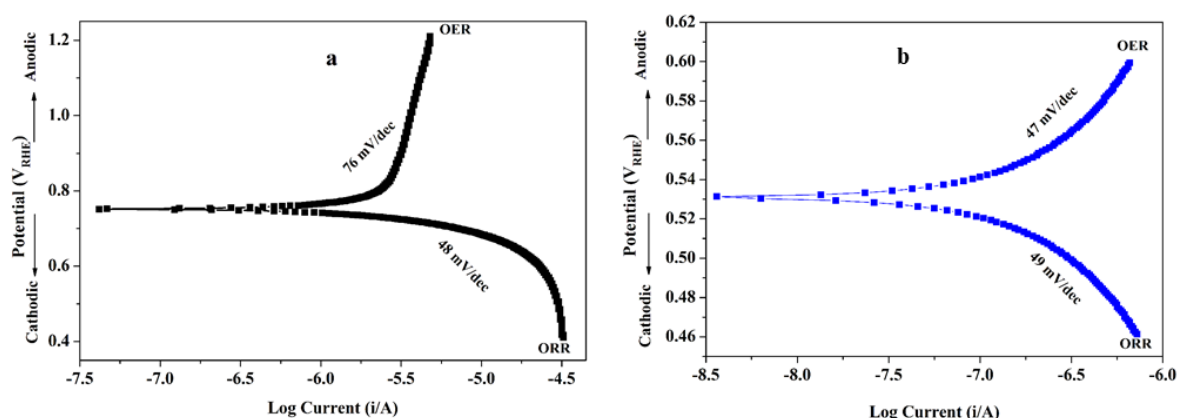

Figure 5. Tafel polarization curves of Ruthenium oxide nanoparticles for OER and ORR in (**a**) air, and (**b**) O_2 saturated atmosphere at 10 mVs^{-1}.

Table 1. Comparison of OER/ORR activity of RuO_2 nanoparticles with other reported literature.

Catalyst	Electrolyte	Scan Rate (mVs^{-1})	Onset Potential (V/RHE)	TafelSlope $(mVdec^{-1})$		Ref.
				OER	ORR	
r-RuO_2	0.1M KOH	10	1.4	-	-	[25]
Ru@RuO_2	0.1M KOH	10	1.3	86	-	[43]
1D-RuO_2-CN_x	0.5M KOH	10	1.42	56	-	[44]
RuO_2	0.05M NaOH	10	1.27	-	-	[45]
$Mn_{25}Ru_{75}$@450	1M NaOH	10	1.4	66	-	[31]
RuO_2 nanoparticles	0.5M KOH	25	1.5	47	49	Present work

The catalytic activity of as-synthesized nanoparticles depends on the concentration of H_2O_2, and the reaction temperature just like that of HRP [33]. The catalytic oxidation of TMB substrate by RuO_2 nanoparticles at a range of H_2O_2 concentration and temperature is shown in Figure 6. It was observed that to attain maximum activity; the RuO_2 nanoparticles required a very high concentration of H_2O_2 (1M) as compared to HRP and on further increasing the concentration of H_2O_2 the catalytic activity was suppressed (Figure 6a). The effect of temperature on the catalytic activity of the RuO_2 nanoparticles was checked in the temperature range of 20–90 °C. Figure 6b indicates that the catalytic activity of RuO_2 nanoparticles increases with the increase in temperature till 60 °C and with further increase in temperature up to 90 °C the activity was quenched. Whereas, HRP shows maximum activity at 30 °C and it shows no activity at higher temperature, i.e., above 60 °C. The as-synthesized nanoparticles showed better activity at a wide range of temperature compared to HRP catalyst. The thermal stability of the RuO_2 nanoparticles and HRP was determined by incubating the reaction mixture with TMB substrate at 80 °C for 90 min, and the aliquots were taken at regular time intervals. It was found that the catalytic activity of RuO_2 nanoparticles was almost preserved until 90 min at 80 °C while the HRP showed no activity in similar reaction conditions (Figure 6c). We have also analyzed the sensitivity of RuO_2 nanoparticles for the detection of H_2O_2 in solution. The aliquots containing different concentration of H_2O_2 and colourimetric reagent were taken and analyzed via spectrophotometry. Figure 6d shows the absorbance at 505 nm, which increases nearly linearly as the concentration of H_2O_2 increased.
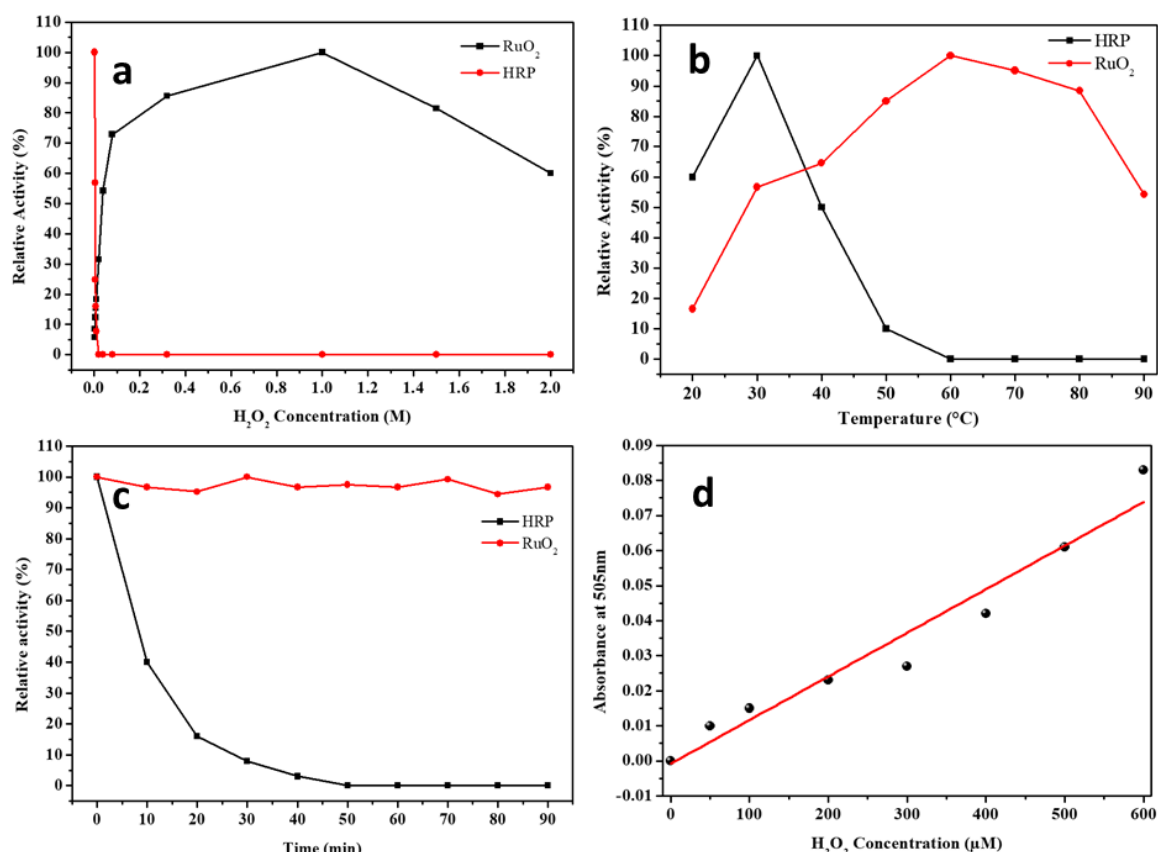
Figure 6. (**a**) H_2O_2 concentration optima and (**b**) temperature optima plots, (**c**) thermal stability (at 80 °C for 90 min under the standard reaction conditions) and (**d**) sensitivity (at 505 nm for the different concentrations of H_2O_2) of ruthenium oxide nanoparticles.

3. Experimental

Ruthenium (III) chloride ($RuCl_3.xH_2O$, Alfa Aesar, Haverhill, MA, USA, 99.9%), NaOH(Merck India Ltd., Mumbai, India), hydrogen peroxide (50% *w/v*, Merck India Ltd.), HRP and Tetramethylbenzidine (SRL, Mumbai, India) were used without further purification. 1.3 mmol of $RuCl_3.xH_2O$ was dissolved in 50 mL of water in a two-neck flask, followed by the dropwise addition of 1.5M aqueous NaOH to a pH ~8. The solution was continuously stirred and refluxed at 80 °C untilthe black precipitate was observed. The black precipitate was collected through centrifugation process and repeatedly washed with double-distilled water followed by ethanol to remove the Cl⁻ ions. The Cl⁻ ions present in the supernatant liquid were checked with the aqueous solution of silver nitrate. The black precipitate was dried at 100 °C in the hot-air oven and grounded to form a fine powder. Further, the black colour powder was annealed at 300 °C for 6 h in a high temperature furnace to obtained black colour ruthenium oxide nanoparticles. The as-synthesized nanoparticles were further employed to study the catalytic activity.

3.1. Physical Characterization

Powder X-ray diffraction (XRD) was performed using a RigakuUltima IV X-ray diffractometer with Ni-filtered Cu-Kα radiation (λ = 1.5416 Å). The morphological features of synthesized ruthenium oxide nanoparticles were determined by Zeiss EVO40 Scanning Electron Microscope (SEM) at an accelerating voltage of 20 kV. Transmission electron microscopic (TEM) analysis was carried out on FEI Technai G^2 20 HRTEM (High Resolution Transmission Electron Microscope) with an accelerating voltage of 200 kV. The surface area and the pore size of as-synthesized nanoparticles were determined using

Brunauer-Emmett-Teller (BET) surface area analyzer (Model: Nova 2000e, Quantachrome Instruments Limited, Boynton Beach, FL, USA) at liquid nitrogen temperature (77K).

3.2. Electrochemical Measurements

The electrolysis of water for OER and ORR was carried out with a three-electrode electrochemical work station (potentiostat/galvanostat, CHI 660E, Shenzhen, China) at room temperature in alkaline medium (0.5 M KOH) to investigate the redox behaviour of the synthesized RuO_2 nanoparticles. Pt wire, Ag/AgCl and glassy carbon electrodes were used as the counter, reference, and working electrodes in the electrochemical analyzer. The reference electrode (Ag/AgCl) was converted to the reversible hydrogen electrode (RHE) as per the conversion equation, i.e., Nernst Equation at 25 °C.

$$E_{RHE} = E_{Ag/AgCl} + 0.059 \text{ pH} + 0.197 \text{ V}$$

The slurry was prepared by sonicating 2.5 mg of catalysts in 0.5 mL of isopropanol with 0.1 mL of Nafion solution for 10 min. Then a drop of the slurry was cast on the surface of glassy carbon and dried at 60 °C in vacuum oven [46,47]. The loaded amount of the nanoparticles was of ~0.30 mg/cm^2 on the GC electrode, and the area of the working electrode was 0.07 cm^2. Freshly prepared electrodes were used for the electrochemical measurements. Cyclic Voltammetry (CV), linear sweep voltammetry (LSV) and Tafel measurements were done by applying redox potential versus Ag/AgCl electrode for OER and ORR at the scan rate of 25 mV s^{-1} in 0.5 M KOH electrolyte at room temperature in air, nitrogen and saturated oxygen atmosphere.

3.3. Catalytic Activity of RuO$_2$ Nanoparticles and HRP

The catalytic activity of as-synthesized nanoparticles and HRP was checked by peroxidase substrate Tetramethylbenzidine (TMB) [48]. In a typical procedure, 200 μL of RuO_2 nanoparticles (2 mg/mL), 1.5 mL TMB, and 5 μL H_2O_2 were added in 1mL of 0.02M acetate buffer (Ph~4.5) and incubated in a water-bath at 30 °C for 10 min and the progress of the reaction was monitored by A Shimadzu UV-2450 spectrophotometer. The leaching of the ions from the reaction mixture was checked by incubating a suspension of RuO_2 nanoparticles in acetate buffer (5 mg/mL, Ph~3.5) (marked as control) for 10 min at 45 °C; the nanoparticles were removed from the reaction mixture, and the catalytic activity of the reaction mixture was analyzed. No activity was found in control. In order to investigate the effect of H_2O_2 concentration on the activity of as-synthesized nanoparticles, it was examined by varying the concentrations of H_2O_2 (0.002–2M). The effect of change of temperature on the activity of RuO_2 nanoparticles was determined by incubating the reaction mixture from 20 to 90 °C. The obtained results were compared with the activity of HRP enzyme over the same range of parameters.

3.4. Detection of H$_2$O$_2$

In a typical experiment, 1 mL hydrogen peroxide (50–600 μM) was added to the 1mLcolourimetric reagent, i.e., 10 mg phenol, 10 mg of 4-aminoantipyrine, 50 mg of RuO_2 nanoparticles, dissolved in 20 mL of 100 mM acetic acid buffer (pH 5.6) [49]. The test tubes containing different concentrations of H_2O_2 and blank, i.e., without H_2O_2 were incubated in a water-bath for 10 min at 30 °C, and the progress of the reaction was monitored by spectrophotometer at 505 nm.

4. Conclusions

We have successfully synthesized the ultrafine ruthenium oxide nanoparticles via a simple co-precipitation method at 300 °C. The application of synthesized nanoparticles was successfully studied, and it was concluded that RuO_2 nanoparticles are an effective bifunctional and stable material for OER and ORR reactions in the air, N_2 and O_2 atmosphere. Also, RuO_2 nanoparticles were used as sensors for the detection of H_2O_2 in a solution. The RuO_2 nanoparticles have a comparable limit of detection and linear dynamic values ranging from 600 to 10 μM of H_2O_2. The economically viable

as-synthesized nanoparticles could be used as an active nonenzymatic electrochemical sensor for the selective detection of H_2O_2. Further, these nanoparticles showed efficient electrocatalytic activity with low energy loss. Tafel slopes were found to be very low and the electrode material was stable as established by CA studies. Therefore, the ruthenium oxide nanoparticles consumed less energy during the water redox reaction (OER and ORR) and proved to be a better electrode material for OER/ORR reactions, showing its excellent potential for further applications in the future.

Author Contributions: R.P. is responsible for the experimental reactions, basic characterization and first draft of the manuscript, M.P. did the detection of H_2O_2 measurements, J.A. did the electrochemical measurement and its discussion, M.S. was the co-supervisor of first author and wrote the discussion part for the detection of H_2O_2 measurements, S.M.A. helps in the editing and electrochemical measurements, N.A. designed the electrochemical set for the water redox reaction and did the primary measurements, M.A.M.K.helps in the discussion and measurements electrochemical studies and T.A. is responsible for supervision, creation ideas, infrastructure, editing and final draft of the manuscript. All authors have read and agreed to the published version of the manuscript.

Conflicts of Interest: The authors declare that there is no conflict of interest.

References

1. Solomonn, S.; Plattner, G.-K.; Knutti, R.; Friedlingstein, P. Irreversible climate change due to carbon dioxide emissions. *Proc. Natl. Acad. Sci. USA* **2009**, *106*, 1704–1709. [CrossRef] [PubMed]

2. Chhow, J.; Kopp, R.J.; Portney, P.R. Energy resources and global development. *Science* **2003**, *302*, 1528–1531. [CrossRef] [PubMed]

3. Ahmad, T.; Lone, I.H.; Ansari, S.G.; Ahmed, J.; Ahamad, T.; Alshehri, S.M. Multifunctional properties and applications of yttrium ferrite nanoparticles prepared by citrate precursor route. *Mater. Des.* **2017**, *126*, 331–338. [CrossRef]

4. Vondrák, J.; Klápště, B.; Velická, J.; Sedlaříková, M.; Ćerný, R. Hydrogen-oxygen fuel cells. *J. Solid State Electrochem.* **2003**, *8*, 44–47. [CrossRef]

5. Zhang, X.; Wang, X.-G.; Xie, Z.; Zhou, Z. Recent progress in rechargeable alkali metal-air batteries. *Green Energy Environ.* **2016**, *1*, 4–17. [CrossRef]

6. Gutsche, C.; Moeller, C.J.; Knipper, M.; Borchert, H.; Parisi, J.; Plaggenborg, T. Synthesis, structure, and electrochemical stability of Ir-decorated RuO_2 nanoparticles and Ptnanorods as oxygen catalysts. *J. Phys. Chem. C.* **2016**, *120*, 1137–1146. [CrossRef]

7. Tseng, H.-W.; Zong, R.; Muckerman, J.T.; Thummel, R. Mononuclear ruthenium (II) complexes that catalyze water oxidation. *Inorg. Chem.* **2008**, *47*, 11763–11773. [CrossRef]

8. Reier, T.; Oezaslan, M.; Strasser, P. Electrocatalytic oxygen evolution reaction (OER) on Ru, Ir, and Ptcatalysts: A comparative study of nanoparticles and bulk materials. *ACS Catal.* **2012**, *2*, 1765–1772. [CrossRef]

9. Karlsson, E.A.; Lee, B.-L.; Åkermark, T.; Johnston, E.V.; Kärkäs, M.D.; Sun, J.; Hansson, Ö.; Bäckvall, J.-E.; Åkermark, B. Photosensitized water oxidation by use of a bioinspired manganese catalyst. *Angew. Chem. Int. Ed.* **2011**, *50*, 11715–11718. [CrossRef]

10. Ellis, W.C.; McDaniel, N.D.; Bernhard, S.; Collins, T.J. Fast water oxidation using iron. *J. Am. Chem. Soc.* **2010**, *132*, 10990–10991. [CrossRef]

11. Alshehri, S.M.; Ahmed, J.; Alhabarah, A.N.; Ahamad, T.; Ahmad, T. Nitrogen doped cobalt ferrite/carbon nanocomposites for supercapacitor application. *ChemElectroChem* **2017**, *4*, 2952–2958. [CrossRef]

12. Coggins, M.; Zhang, K.M.T.; Chen, Z.; Song, N.; Meyer, T.J. Single-site copper (II) water oxidation electrocatalysis: Rate enhancements with HPO_4^{2-} as a proton acceptor at pH-8. *Angew. Chem. Int. Ed. Engl.* **2014**, *53*, 12226–12230. [CrossRef] [PubMed]

13. Alshehri, S.M.; Ahmed, J.; Ahamad, T.; Alhokbany, N.; Arunachalam, P.; Al-Mayouf, A.M.; Ahmad, T. Synthesis, characterization, multifunctional electrochemical (OGR/ORR/SCs) and photodegradable activities of ZnWO₄ nanobricks. *J. Sol-Gel Sci. Technol.* **2018**, *87*, 137–146. [CrossRef]

14. Fang, Y.-H.; Liu, Z.-P. Mechanism and tafel lines of electro-oxidation of water to oxygen on RuO₂ (110). *J. Am. Chem. Soc.* **2010**, *132*, 18214–18222. [CrossRef]

15. Michas, A.; Andolfatto, F.; Lyons, M.E.G.; Durand, R. Gas evolution reactions at conductive metallic oxide electrodes for solid polymer electrolyte water electrolysis. *Key Eng. Mater.* **1992**, *535*, 72–74. [CrossRef]

16. Cui, X.; Zhou, J.; Ye, Z.; Chen, H.; Li, L.; Ruan, M.; Shi, J. Selective catalytic oxidation of ammonia to nitrogen over mesoporous CuO/RuO₂ synthesized by co-nanocasting-replication method. *J. Catal.* **2010**, *270*, 310–317. [CrossRef]

17. Seki, K. Development of RuO₂/Rutile-TiO₂ catalyst for industrial HCl oxidation process. *Catal. Surv. Asia* **2010**, *14*, 168–175. [CrossRef]

18. Liu, H.; Iglesia, E. Selective oxidation of methanol and ethanol on supported ruthenium oxide clusters at low temperatures. *J. Phys. Chem. B* **2005**, *109*, 2155–2163. [CrossRef]

19. Ma, H.; Liu, C.; Liao, J.; Su, Y.; Xue, X.; Xing, W. Study of ruthenium oxide catalyst for electrocatalytic performance in oxygen evolution. *J. Mol. Catal. A-Chem.* **2006**, *247*, 7–13. [CrossRef]

20. Kiele, N.M.; Herrero, C.; Ranjbari, A.; Aukauloo, A.; Grigoriev, S.A.; Villagra, A.; Millet, P. Ruthenium-based molecular compounds for oxygen evolution in acidic media. *Int. J. Hydrogen Energy* **2013**, *38*, 8590–8596. [CrossRef]

21. Jeon, H.S.; Permana, A.D.C.; Kim, J.; Min, B.K. Water splitting for hydrogen production using a high surface area RuO₂ electrocatalyst synthesized in supercritical water. *Int. J. Hydrogen Energy* **2013**, *38*, 6092–6096. [CrossRef]

22. Tilley, S.D.; Schreier, M.; Azevedo, J.; Stefik, M.; Grätzel, M. Ruthenium oxide hydrogen evolution catalysis on composite cuprous oxide water-splitting photocathodes. *Adv. Funct. Mater.* **2014**, *24*, 303–311. [CrossRef]

23. Ryden, W.D.; Lawson, A.W.; Sartain, C.C. Temperature dependence of the resistivity of RuO₂ and IrO₂. *Phys. Lett.* **1968**, *26*, 209–210. [CrossRef]

24. Hu, J.-M.; Zhang, J.-Q.; Cao, C.-N. Oxygen evolution reaction on IrO₂-based DSA®type electrodes: Kinetics analysis of tafel lines and EIS. *Int. J. Hydrogen Energy* **2004**, *29*, 791–797. [CrossRef]

25. Lee, Y.; Suntivich, J.; May, K.J.; Perry, E.E.; Shao-Horn, Y. Synthesis and activities of rutile IrO₂ and RuO₂ nanoparticles for oxygen evolution in acid and alkaline solutions. *J. Phys. Chem. Lett.* **2012**, *3*, 399–404. [CrossRef]

26. Ahmed, J.; Mao, Y. Ultrafine iridium oxide nanorods synthesized by molten salt method toward electrocatalytic oxygen and hydrogen evolution reactions. *Electrochim. Acta* **2016**, *212*, 686–693. [CrossRef]

27. Chen, Y.M.; Korotcov, A.; Hsu, H.P.; Huang, Y.S.; Tsai, D.S. Raman scattering characterization of well-aligned RuO₂ nanocrystals grown on sapphire substrates. *New J. Phys.* **2007**, *9*, 1–11. [CrossRef]

28. Shen, W.; Shi, J.; Chen, H.; Gu, J.; Zhu, Y.; Dong, X. Synthesis and CO oxidation catalytic character of high surface area ruthenium dioxide replicated by cubic mesoporous silica. *Chem. Lett.* **2005**, *34*, 390–391. [CrossRef]

29. Ryan, J.V.; Berry, A.D.; Anderson, M.L.; Long, J.W.; Stroud, R.M.; Cepak, V.M.; Browning, V.M.; Rolison, D.R.; Merzbacher, C.I. Electronic connection to the interior of a mesoporous insulator with nanowires of crystalline RuO₂. *Nature* **2000**, *406*, 169–172. [CrossRef]

30. Viswanathamurthi, P.; Bhattarai, N.; Kim, C.K.; Kim, H.Y.; Lee, D.R. Ruthenium doped TiO₂ fibers by electrospinning. *Inorg. Chem. Commun.* **2004**, *7*, 679–682. [CrossRef]

31. Browne, M.P.; Nolan, H.; Duesberg, G.S.; Colavita, P.E.; Lyons, M.E.G. Low-overpotential high-activity mixed manganese and ruthenium oxide electrocatalysts for oxygen evolution reaction in alkaline media. *ACS Catal.* **2016**, *6*, 2408–2415. [CrossRef]

32. Gustafson, K.P.J.; Shatskiy, A.; Verho, O.; Kärkäs, M.D.; Schluschass, B.; Tai, C.-W.; Åkermark, B.; Bäckvall, J.-E.; Johnston, E.V. Water oxidation mediated by ruthenium oxide nanoparticles supported on siliceous mesocellular foam. *Catal. Sci. Technol.* **2017**, *7*, 293–299.

33. Gao, L.; Zhuang, J.; Nie, L.; Zhang, J.; Zhang, Y.; Gu, N.; Wang, T.; Feng, J.; Yang, D.; Perrett, S.; et al. Intrinsic peroxidase-like activity of ferromagnetic nanoparticles. *Nat. Nanotechnol.* **2007**, *2*, 577–583. [CrossRef] [PubMed]

34. Chen, X.; Zhou, X.; Hu, J. Pt-DNA complexes as peroxidase mimetics and their applications in colorimetric detection of H_2O_2 and glucose. *Anal. Methods* **2012**, *4*, 2183–2187. [CrossRef]

35. Chen, T.; Tian, L.; Chen, Y.; Liu, B.; Zhang, J. A facile one-pot synthesis of Au/Cu_2O nanocomposites for nonenzymatic detection of hydrogen peroxide. *Nanoscale Res. Lett.* **2015**, *10*, 935. [CrossRef] [PubMed]

36. Guan, J.; Peng, J.; Jin, X. Synthesis of copper sulfide nanorods as peroxidase mimics for the colorimetric detection of hydrogen peroxide. *Anal. Methods* **2015**, *7*, 5454–5461. [CrossRef]

37. Wei, Y.; Zhang, Y.; Liu, Z.; Guo, M. A Novel Profluorescent Probe for detecting oxidative stress induced by metal and H_2O_2 in living cells. *Chem. Commun.* **2010**, *46*, 4472–4474. [CrossRef]

38. Dickinson, B.C.; Chang, C.J. A targetable fluorescent probe for imaging hydrogen peroxide in the mitochondria of living cells. *J. Am. Chem. Soc.* **2008**, *130*, 9638–9639. [CrossRef]

39. Finkel, T.; Serrano, M.; Blasco, M.A. The common biology of cancer and ageing. *Nature* **2007**, *448*, 767–774. [CrossRef]

40. Bard, A.J.; Faulkner, L.R. *Electrochemical Methods: Fundamentals and Applications*, 2nd ed.; John Wiley & Sons: New York, NY, USA, 2001.

41. Stoerzinger, K.A.; Qiao, L.; Biegalski, M.D.; Shao-Horn, Y. Orientation-dependent oxygen evolution activities of rutile IrO_2 and RuO_2. *J. Phys. Chem. Lett.* **2014**, *5*, 1636–1641. [CrossRef]

42. AlShehri, S.M.; Ahmed, J.; Ahamad, T.; Arunachalam, P.; Ahmad, T.; Khan, A. Bifunctional electro-catalytic performances of $CoWO_4$ nanocubes for water redox reactions (OER/ORR). *RSC Adv.* **2017**, *7*, 45615–45623. [CrossRef]

43. Jiang, R.; Tran, D.T.; Li, J.; Chu, D. $Ru@RuO_2$ core-shell nanorods: A highly active and stable bifunctional catalyst for oxygen evolution and hydrogen evolution reactions. *Energy Environ. Mater.* **2019**, *2*, 201–208. [CrossRef]

44. Bhowmik, T.; Kundu, M.K.; Barman, S. Growth of one-dimensional RuO_2 nanowires on g-carbon nitride: An active and stable bifunctional electrocatalyst for hydrogen and oxygen evolution reactions at all pH values. *ACS Appl. Mater. Inter.* **2016**, *8*, 28678–28688. [CrossRef] [PubMed]

45. Cherevko, S.; Geiger, S.; Kasian, O.; Kulyk, N.; Grote, J.-P.; Savan, A.; Shrestha, B.R.; Merzlikin, S.; Breitbach, B.; Ludwig, A.; et al. Oxygen and hydrogen evolution reactions on Ru, RuO_2, Ir, and IrO_2 thin film electrodes in acidic and alkaline electrolytes: A comparative study on activity and stability. *Catal. Today* **2016**, *262*, 170–180. [CrossRef]

46. Farooq, U.; Phul, P.; Alshehri, S.M.; Ahmed, J.; Ahmad, T. Electrocatalytic and enhanced photocatalytic applications of sodium niobate nanoparticles developed by citrate precursor route. *Sci. Rep.* **2019**, *9*, 4488. [CrossRef]

47. Ahmed, J.; Ubaidullah, M.; Ahmad, T.; Alhokbany, N.; Alshehri, S.M. Synthesis of graphite oxide/cobalt molybdenum oxide hybrid nanosheets for enhanced electrochemical performances in supercapacitors and OER. *ChemElectroChem* **2019**, *6*, 2524–2530. [CrossRef]

48. Bos, E.S.; van der Doelen, A.A.; van Rooy, N.; Schuurs, A.H.W.M. 3,3′,5,5′-etramethylbenzidine as an ames test negative chromogen for horse-radish peroxidase in enzyme immunoassay. *J. Immunoass.* **1981**, *2*, 187–204. [CrossRef]

49. Zhou, B.; Wang, J.; Guo, Z.; Tan, H.; Zhu, X. A simple colorimetric method for determination of hydrogen peroxide in plant tissues. *Plant Growth Regul.* **2006**, *49*, 113–118. [CrossRef]